ICAS Paper No. 70–03

EXPERIMENTAL AND THEORETICAL INVESTIGATIONS OF DIFFERENT CONFIGURATIONS OF LIFTING RE-ENTRY VEHICLES IN HYPERSONIC LOW DENSITY FLOW

by
G. Koppenwallner, Deputy Department Chief
and
W. Wuest, Director of Space-Aerodynamics Department
DFVLR/AVA Göttingen, Germany

The Seventh Congress of the International Council of the Aeronautical Sciences

CONSIGLIO NAZIONALE DELLE RICERCHE, ROMA, ITALY / SEPTEMBER 14-18, 1970

Price: 400 Lire

EXPERIMENTAL AND THEORETICAL INVESTIGATIONS OF DIFFERENT CONFIGURATIONS OF LIFTING RE-ENTRY VEHICLES IN HYPERSONIC LOW DENSITY FLOW

G. Koppenwallner and W. Wuest
Deutsche Forschungs- und Versuchsanstalt für Luft- und Raumfahrt
Aerodynamische Versuchsanstalt Göttingen, Germany

Abstract

Pressure distribution, force and heat transfer measurements on different lifting re-entry vehicles (blunted half-elliptical cones, delta wing, cylindrical cone) are reported. The measurements which included also the hinge moments of control surfaces, have been done in the hypersonic low density wind tunnel of the Aerodynamische Versuchsanstalt Göttingen in the Mach number range 8 + 22 and Reynolds number range 10 000 to 40 000. The experimental results are compared with calculations obtained by different methods.

I. Introduction

When a space vehicle approaching the earth from space or orbit encounters the atmosphere, a shock wave will form ahead of the nose and as it plunges into increasingly deeper and denser atmosphere the vehicle's kinetic energy will be continuously converted into heat. This first step of the reentry may be simulated rather satisfactorily in a hypersonic low density tunnel. The necessary high gas velocities may be produced by expanding a heated gas in a nozzle. A rather large range of available stagnation pressures should be provided. It is obvious that special measuring techniques must be applied because of the low density and the high stagnation temperatures. For flow visualization the familiar Schlieren or interferometric technique fails, but a high frequency glow discharge technique or the electron beam technique are efficient substitutes. The measurement of pressure distribution requires very sensitive indicators and long running time of the wind tunnel, different systems of force balances are necessary to cover the large range of forces and transient technique are needed for heat transfer measurements.

Experimental results are obtained for various forms of lifting reentry bodies which are generally deduced from an elliptical half cone. These results may be compared with measurements on more basic shapes such as sphere, cylindrical cone and delta wing or with theoretical results obtained by the modified Newton's theory or by the free molecular flow theory.

II. Experimental set up

Hypersonic low density wind tunnel of the AVA Göttingen

A hypersonic low density wind tunnel designed for Mach numbers between 7 and 25 and stagnation temperatures up to 3 000 ^{o}K or even higher has been taken into operation at the Aerodynamische Versuchsanstalt Göttingen (DFVLR) during the last years [1, 2, 3]. The complete facility comprises three test sections, two of which are connected with the same multistage system of large Roots-pumps (Fig. 1) and operate at Mach numbers from 7 to 25 with stagnation pressures from 5 to 500 atm and with heating by graphite or resistance heaters. The third test section (Fig. 2) is designed for a lower density level and operates with two independent pumping systems (water cooled oil diffusion pump and oil vapor stream pump) allowing the application of the skimmer technique for producing a molecular beam.

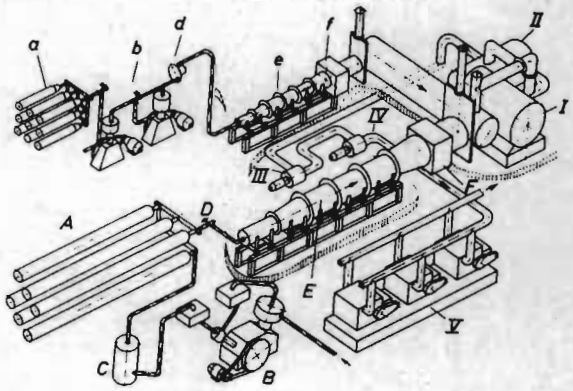

Figure 1. Hypersonic low density wind tunnel of the Aerodynamische Versuchsanstalt Göttingen. a-f test section I, A-F test section II, a, A gas reservoir, b, B two-stage compressor, C dryer, d, D pressure regulator, e, E test section with heater, nozzle test chamber and diffusor, f, F cooler, I-V five stage vacuum pumping system.

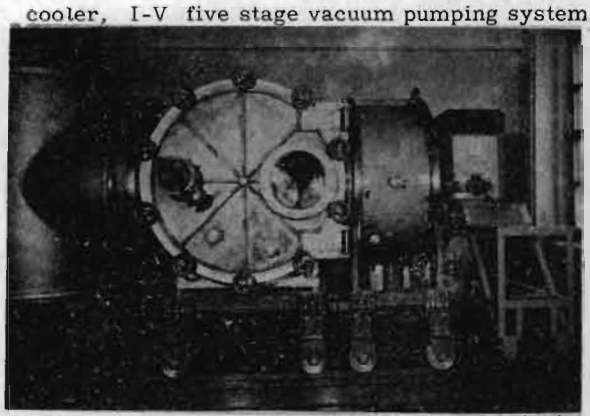

Figure 2. High vacuum wind tunnel of the AVA Göttingen (DFVLR)

Measuring technique

Flow visualization

Flow visualization by Schlieren technique or interferometry breaks down because of the low density. Stable images of high intensity are obtained by high frequency glow discharge (see Fig. 8/9). More details of the density field may be detected by sweeping an electron beam which has also the advantage that sectional views may be obtained and therefore three dimensional studies are possible [4].

Pressure measurements

The measurement of pressure distributions on bodies in rarefied flow is complicated because of the low pressure level and the time lag in the pressure connections. Further difficulties arise from necessary corrections because of thermal transpiration, viscosity effects and sensitivity to the geometry of pressure holes. An extended program of basic studies on pressure measuring technique in rarefied hypersonic flow is therefore in progress [5].

Force measurements

As it is often desired to cover an utmost extended Reynolds number range from continuum flow to free molecule flow the range of possible forces, too, is extremely extended. For larger forces built-in strain gauge balances are most convenient, but for small forces sensitive electrodynamic balances are needed. Most force measurements have been done with a three-components strain gauge balance with a lift and drag range of 30 pond (Fig. 3) [6]. The balance must of course

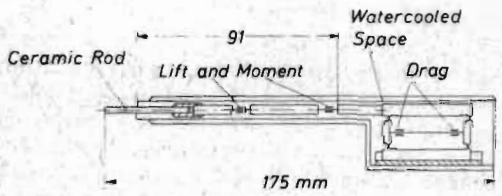

Figure 3. Water-cooled three-components balance with strain gauges

be prevented from the high enthalpy flow and is therefore inserted in a water cooled housing. An accuracy of $\pm 1\,^{o}/o$ for lift and $\pm 3\,^{o}/o$ for drag was obtained. For measuring very small forces with ranges varying from 10 µp to 0.2 p a commercial vacuum microbalance is used, which has a sensitivity of 0.1 µp and which is wellsuited for measurements in free molecular flow.

Heat transfer measurement

Two different transient techniques have been used for measuring heat transfer rates in hypersonic rarefied flow. In the first case the model is thin-walled and made by electroforming. Vacuum-coating of thermoelements on the surface allow local heat transfer measurements. Integral heat transfer rate is measured with a solid model made from a material of high conductivity. This method needs only one single thermoelement and is often preferred for its simplicity although it gives less detailed information. In both methods retractable heat shields are used, which expose the model only for a short time interval to the hypersonic high enthalpy flow. Differentiation of the temperature rise with respect to time by electronic means give a direct measure of heat transfer rate. So far heat transfer rates were measured only on basic shapes, especially cylinders [6], in a very large range of rarefaction, but an extension to reentry bodies is planned in the near future.

Description of the models

Technique of manufacturing the models

In most cases thin-walled models were used in order to reach constant temperature in short time and for reducing the weight. Electroforming of the models proved to be the most convenient technique [8]. Stainless steel is generally used as core material, if the core is retractable. In other cases cores are made from metals with low melting point (Ferrotru), which must be melted out after electroplating. Only for measuring total heat transfer rates solid models are used.

Lifting reentry bodies

"Integral Body" of Junkers

The "Integral Body" is essentially a blunted elliptical half cone. The name indicates that production of lift and taking up cargo is incorporated in one single body. The half angles of the basic elliptic cone are 11^{o} and 15.5^{o}. The main dimensions are given in Fig. 4. At the rear end the cone is flattened and equipped with two flaps outside the span or with two flaps at the upper and lower trailing edge within span. Different models have been used for pressure measurements on the upper- and lowerside, for force measurements and for measurements of hinge moments of the outside flaps. The pressure measurement models were cooled with oil of low viscosity introduced at low pressure in order to avoid bending of the plane surface. The model with the outside flaps and the built in moment gauge (see Fig. 4 dashed line) could not be cooled.

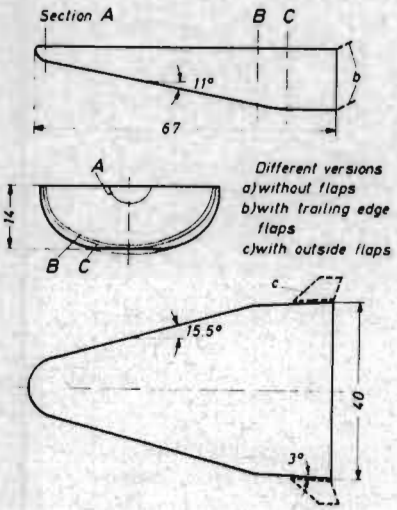

Figure 4. Integral Body of Junkers

"Lifting Body LB10" of ERNO

The "Lifting Body LB10" (Fig. 5) has the same basic concept, but with larger bluntness ratio and two vertical tails.

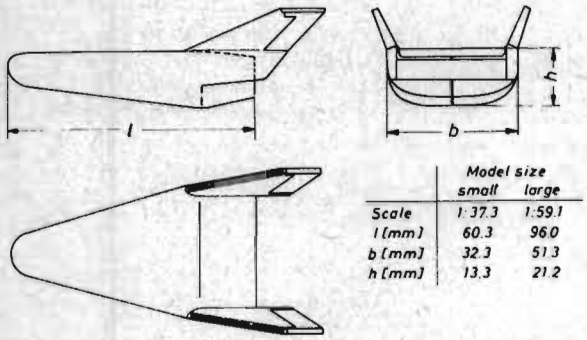

	Model size small	large
Scale	1:37.3	1:59.1
l [mm]	60.3	96.0
b [mm]	32.3	51.3
h [mm]	13.3	21.2

Figure 5. Lifting Body LB10 of ERNO

Delta wing

This model, which is shown in Fig. 6, has sharp leading edges contrary to the lifting bodies.

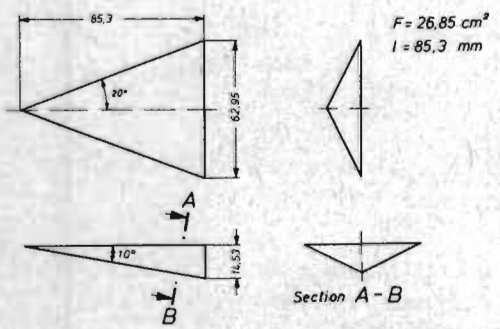

Figure 6. Delta wing

Conical bodies

All four conical bodies (Fig. 7) have a half cone angle of 10° but a different length. The tips are pointed with a radius of less than 0.1 mm. Two of the conical bodies have a cylindrical part of two diameters length.

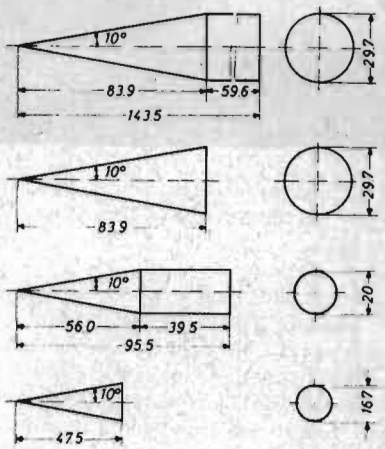

Figure 7. Conical bodies

III. Experimental results

Flow visualization and flowfield measurements

The high-frequency glow discharge method, described in II. has been used to visualize the shock-wave pattern around an "Integral Body" (Fig. 8) at a Mach number Ma = 7.5, Reynolds numbers ranging from $8 \cdot 10^3$ to $4.5 \cdot 10^4$ and different angles of attack [9]. Similar measurements were made with the "Lifting Body" of ERNO (Fig. 9) [10].

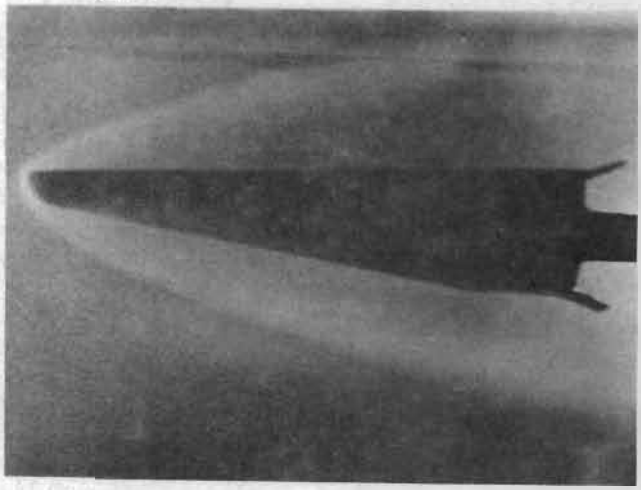

Figure 8. Shock wave pattern around an Integral Body visualized by glow discharge.

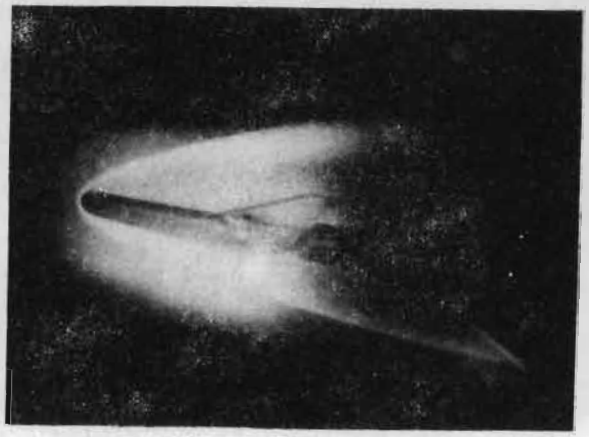

Figure 9. Shock wave pattern around an Lifting Body LB10 of ERNO visualized by glow discharge.

Pitot pressure traverses around the Integral Body at zero angle of attack in the Reynolds number range 10 000 to 31 600 and at a Mach number Ma = 20 analyzed the shock layer. In short distance of the outside flap the pitot pressure is much smaller than in the flowfield outside of the shock wave as is seen in Fig. 10. It can be recognized that small flaps are ineffective to produce noticeable control forces.

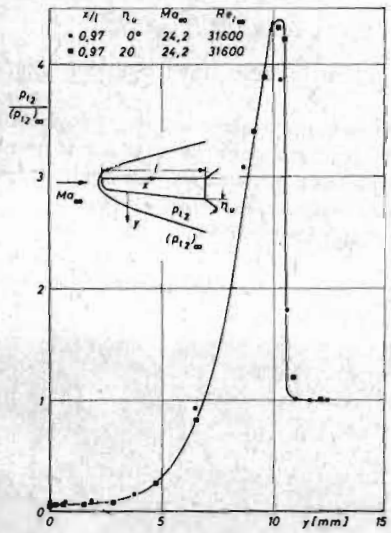

Figure 10. Pitot pressure traverses around an Integral Body.

Pressure distribution on "Integral Body"

Lower side

Fig. 11 and 12 show the pressure distribution on the centre-line at two different Reynolds numbers with or without incidence angle of the trailing edge flaps. It may be recognized that Reynolds number has a strong influence on the pressure distribution at small or negative angles of incidence of the integral body. With decreasing Reynolds number the boundary layer thickness increases with consequent rise of the pressure. The trailing edge

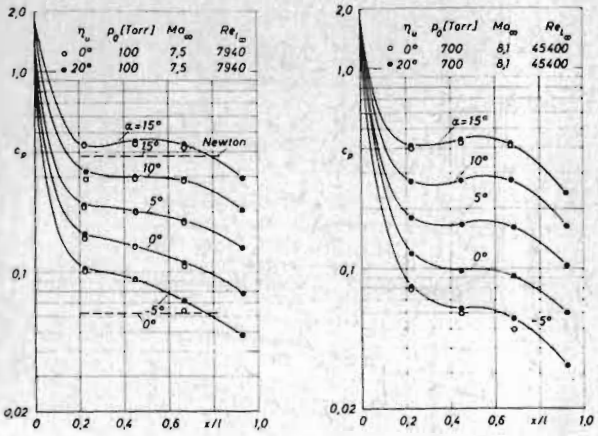

Figure 11/12. Pressure distribution measured on the lower-side centre-line of an Integral Body at $Ma_\infty = 7$ and Re = 7 940 (left) or Re = 45 400 (right).

flaps seem to have no influence on the pressure distribution. Similar measurements were done at a Mach number 20 but show no appreciable difference in comparison to the measurements at Ma = 7.

The pressure distribution on a meridian line shows good agreement with Newtonian theory for angles of attack $\geq 5^\circ$, but large deviations for smaller angles (Fig. 13). Measurements at different distances from the tip show that these deviations increase when approaching the tip.

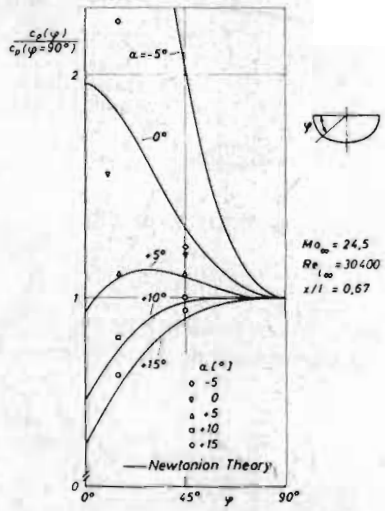

Figure 13. Pressure distribution on a meridian line of an Integral Body at $Ma_\infty = 24.5$ and Re = 30 400.

The hinge moments of the lateral flaps (see Fig. 4) were measured for different flap angles and different angles of attack. Fig. 14 shows a strong influence of Reynolds number on the hinge moments.

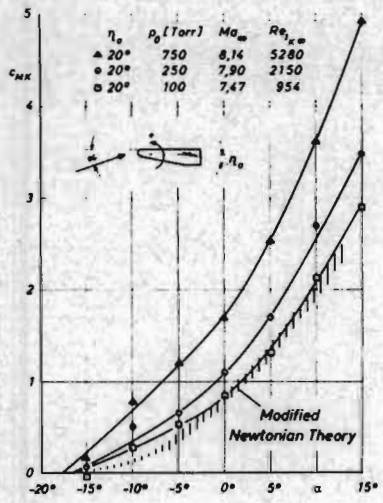

Figure 14. Hinge moments of outer flaps for a flap angle $\eta_a = 20^\circ$ and different incidence angles of the Integral Body.

Upper side

Although according to Newton's theory the pressure should be constant along the plane upper side, the measurements (Fig. 15) show a large pressure gradient and the pressure level is essentially higher than in Newton's case. The pressure gradient may be caused by rounding the nose and by the displacement thickness of the boundary layer. Contrarily to the lower side the pressure distribution is influenced by an angle of incidence of the trailing edge flaps at Mach number Ma = 7.5 but not at a Mach number Ma = 24.5. In spanwise direction, too, the pressure is not constant but increases to the edges for negative angles of attack, but decreases for positive angles of attack (Fig. 16).

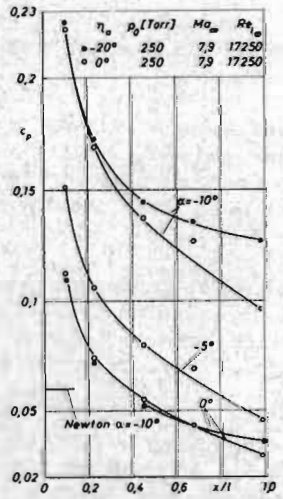

Figure 15. Pressure distribution on the flat upper side of an Integral Body at $Ma_\infty = 7.9$ and $Re_{l\infty} = 17\,250$.

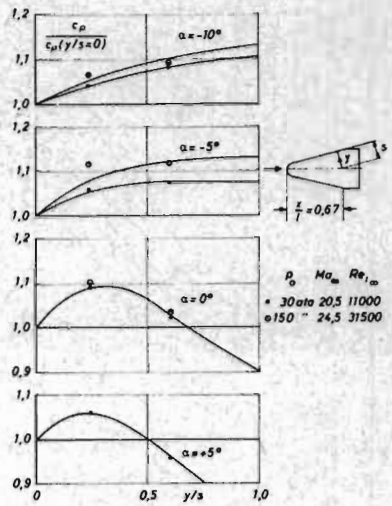

Figure 16. Spanwise pressure distribution on the flat upper-side of an Integral Body at $Ma_\infty = 20 - 24$.

Force measurements on various reentry vehicles with and without flaps

Integral Body of Junkers [6]

The measured lift coefficient (Fig. 17) is independent from Mach and Reynolds number in the range of investigation, which covers Reynolds numbers from Re = 9 780 to Re = 40 600 and Mach numbers Ma = 7 to 22. The drag coefficient, however, depends on Reynolds and Mach number as is shown in Fig. 18.

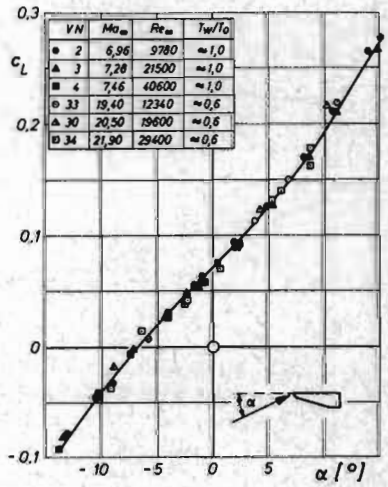

Figure 17. Lift coefficient of Integral Body for various Mach- and Reynolds numbers.

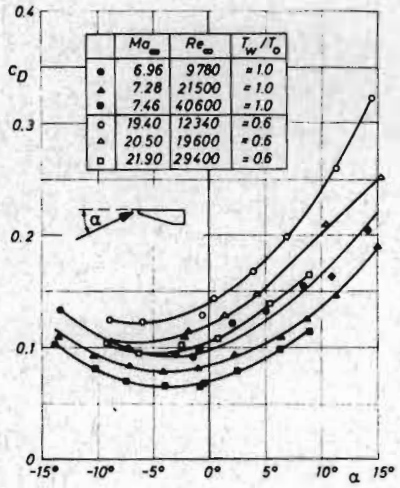

Figure 18. Drag coefficient of Integral Body for various Mach- and Reynolds numbers.

Lifting Body LB10 of ERNO [10]

A representative result from the measurements on the lifting body LB10 of ERNO is given in Fig. 19. It is easily seen, that the larger bluntness of the latter configuration results in larger drag. The two vertical tails have no influence on lift coefficient but on drag and moment coefficients.

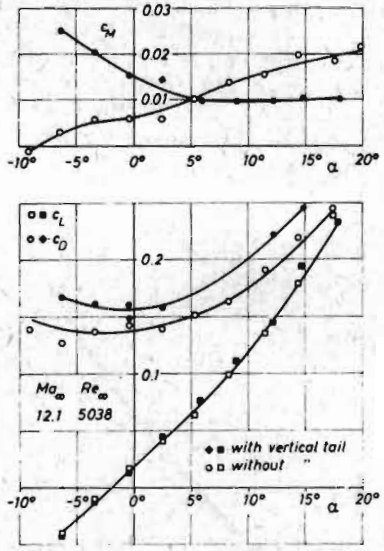

Figure 19. Representative results on Lifting Body LB10 of ERNO with and without vertical tails.

Force measurements on simple shapes

A cone with 10^o half angle was investigated at different Mach- and Reynolds numbers. The measured lift coefficient (Fig. 20) decreases with increasing Mach number when compared with the lift coefficient calculated by Newton's theory. The drag coefficient, however, becomes larger with increasing rarefaction parameter $Ma_\infty/\sqrt{Re_\infty}$ as is shown in Fig. 21. As the same figure also contains the drag of a cone-cylinder, the friction drag of a cylinder may be deduced by subtracting both curves.

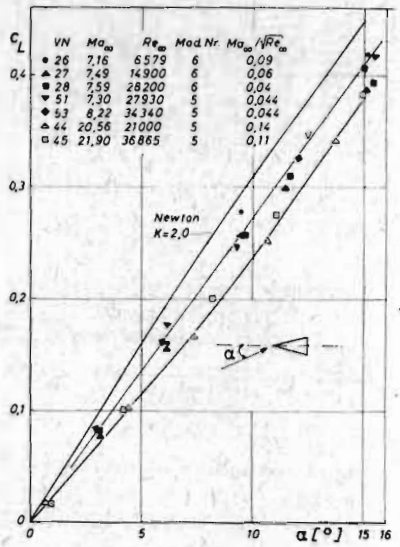

Figure 20. Lift coefficient of cones for various Mach- and Reynolds numbers.

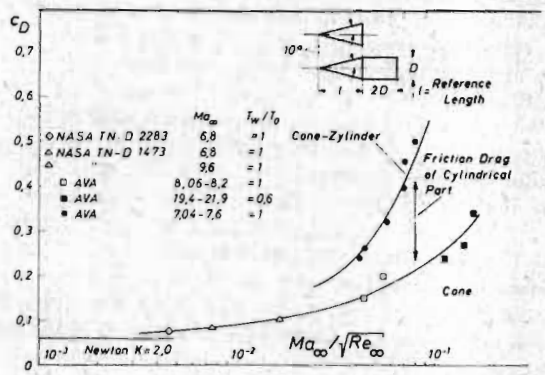

Figure 21. Drag coefficient of cones and cone-cylinders in dependance from rarefaction parameter.

During the measurements it was recognized that in the hypersonic test section with conical nozzle a radial flow is produced and corrections must be applied in order to eliminate the influence of radial flow (see IV).

The investigated delta wing has sharp leading edges and therefore small drag. The lift is not dependent of Mach- or Reynolds number. The lift to drag ratio (Fig. 22) is larger than for the integral body or cone.

As an example for a blunt body the sphere drag was investigated in the whole range from continuum flow to free molecule flow (Fig. 23). Near the free molecule flow regime the friction drag is essentially

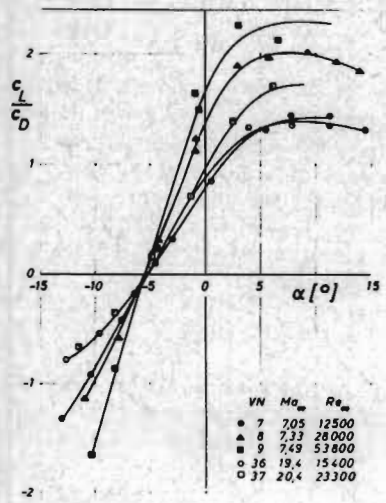

Figure 22. Lift to drag ratio of a delta wing at different Mach- and Reynolds numbers.

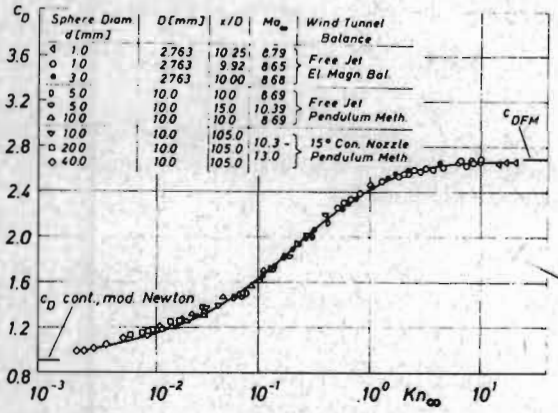

Figure 23. Drag of uncooled spheres in the whole range from continuum to free molecule flow.

dependent of the surface temperature. The measurements have only been done with uncooled spheres and consequently with high friction drag, so that no maximum of drag coefficient is perceptible as would be expected for cooled spheres. Further measurements on cooled spheres are therefore planned.

An interesting correlation of the lift to drag ratio to the rarefaction parameter $Ma_\infty/\sqrt{Re_\infty}$ is shown in Fig. 24. It is shown, that different reentry bodies follow the same curve whereas the cone is more sensitive to rarefaction.

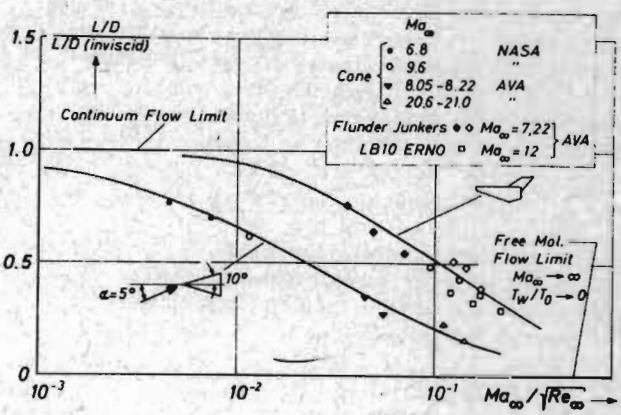

Figure 24. Decrease of lift to drag ratio with increasing rarefaction for cones and reentry bodies.

Heat transfer measurements

Heat transfer measurements covering the whole range from continuum flow to free molecule flow have been done on simple shapes such as cylinders [7]. According to Fig. 25 a smooth transition from continuum flow to free molecule flow Nusselt number is obtained. A similar behaviour is expected for reentry bodies and further measurements are planned.

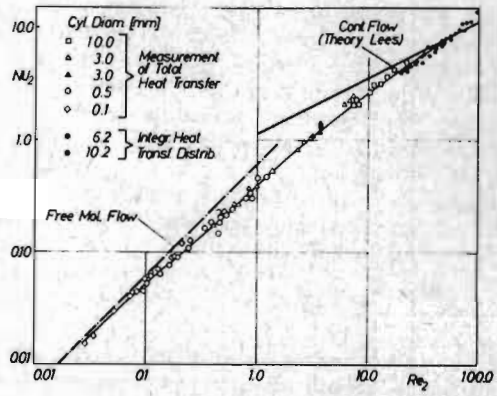

Figure 25. Total heat transfer on cylinders in the whole range from free molecule to continuum flow.

IV. Comparison with theoretical results

A calculation of forces and moments is possible in the limiting cases of free molecule flow and for hypersonic continuum flow on the basis of the simple Newtonian theory. An essential feature of both theories is the fact that pressure may be calculated from local conditions. It is hoped that this simplification will also be true for the whole intermediate range of rarefaction. However more informations on surface pressure and frictional stress are needed for the complete range of Knudsen numbers from continuum to free molecular

flow and various degrees of surface cooling. Work is this field is in progress. In wind tunnel tests with conical nozzles or free jets one has usually no parallel but rather a radial flow. For the processing of wind tunnel data the corrections, caused by radial flow, must be known.

Free molecule flow theory

With the molecular Mach number $S = \sqrt{\gamma/2} \cdot Ma$ and δ the angle between the normal to the surface element and the incident flow on gets for the hypersonic limit $S \cdot \cos\delta \gg 1$ the formula

$$p = \varrho V^2 [(2 - \sigma') \cos^2\delta + \frac{\sigma'}{2} \sqrt{\frac{\pi T_w}{T}} \frac{\cos\delta}{S}] \qquad (1)$$

$$\tau = \sigma \varrho V^2 \sin\delta \cos\delta \qquad (2)$$

$$Q = \alpha \varrho (RT)^{3/2} \sqrt{2} S \cos\delta [S^2 - \frac{\varkappa + 1}{2(\varkappa - 1)} \frac{T_w}{T}] \qquad (3)$$

with σ', σ, α respectively normal and tangential momentum and thermal accommodation coefficient.

For diffuse reflexion ($\sigma' = 1$) and cold wall ($T_w \rightarrow 0$) formula (1) identical with Newton's law, and it is obvious that the difference between the free molecular theory and Newton's theory lies in the occurence of the wall temperature term, caused by the diffusively reflected molecules and the nonzero friction stress. Moreover the free molecular flow theory gives information on heat transfer. If the body contour and the wind vector is given analytically, the forces and moments acting on the body, may be easily calculated by numerical integration. In the hypersonic approximation the shadow parts of the body have zero pressure so that

$$\cos^2\delta \equiv 0 \quad \text{for} \quad \underline{n} \cdot \underline{v} < 0 \qquad (4)$$

where $\underline{n}$ is the normal vector and $\underline{v}$ the wind vector. Some difficulties arise in determining the direction $\underline{h}$ of shear stress for given $\underline{n}$ and $\underline{v}$. According to WUEST [12] the direction $\underline{g}$ on the surface element perpendicular to the incident flow must be introduced and $\underline{h}$ is determined by the conditions

$$(\underline{v} \cdot \underline{g}) = (\underline{n} \cdot \underline{g}) = (\underline{n} \cdot \underline{h}) = (\underline{g} \cdot \underline{h}) = 0 . \qquad (5)$$

Modified Newton's theory

It was first recognized by EPSTEIN 1931 that, in hypersonic flow the conditions behind a shock are equivalent with Newton's concept of flow resistance and the pressure coefficient may be expressed by

$$c_p = \frac{p_s - p_\infty}{\varrho_\infty V^2/2} = k \cdot \cos^2\delta \qquad (6)$$

where $k = 2$ in Newton's concept. It is obvious to adjust k so as to get $c_p = c_{p_o}$ in the stagnation point (modified Newton's theory) Newton's law does not consider any friction drag and fails also in determining the pressure coefficient, if $\cos\delta$ approaches zero. An empiric modification to improve this situation was given by WIDJAJA et al [13] with the formula

$$c_p = k [(1 - \xi) \cos\delta + \xi]^2 \qquad (7)$$

where $\xi = 0.1$ fits satisfactory the measured values. Comparisons of measured data with Newtonian theory may be found in Fig. 11, 13, 14 and 20.

Hypersonic radial flow

In radial flow the direction of the incident flow is not constant as in parallel flow and the density changes with distance from the source.

In the continuity equation

$$\varrho v = \text{const}/r^2$$

v becomes constant for sufficient distance from the source so that

$$\varrho = \text{const}/r^2$$

and one gets in the regime of Newton's theory

$$c_p = k \frac{r_o^2}{r^2} \cos^2\delta = k \frac{r_o^2}{r^2} \cos^2(\vartheta + \varphi) \qquad (8)$$

where r_o is a reference distance and ϑ the angle between the normal of the surface element to parallel flow direction and φ the angle between parallel flow and radial flow direction. Formula (8) has been exploited to calculate radial flow corrections for different shapes used in the experiments [12]. As representative result Fig. 26 shows the lift coefficient rise $\partial c_L/\partial\alpha$ for a cone with various distances from the source and different cone angles.

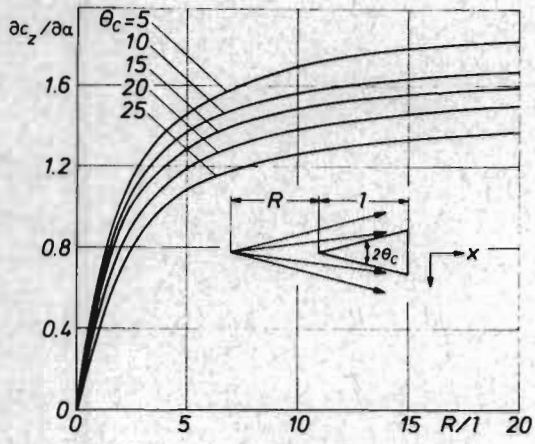

Figure 26. Effect of radial flow on lift coefficient rise of cones with different cone angles.

V. Conclusions

1) The pressure distributions shows good agreement with Newtonian theory for suffiently large angles between surface and flow ($> 15^{\circ}$).

2) The lift coefficient follows very satisfactorily the Newtonian theory.

3) The moment coefficient is more sensitive to shockwave boundary layer interference and Newtonian theory may only give a qualitative representation.

4) For the calculation of drag the boundary layer displacement effects and for high rarefaction also the diffusive reflection of molecules must be taken into account.

5) The wind tunnel data must be corrected for possible radial flow, considering deviations in flow direction and density gradient.

VI. References

[1] FLECKEN, F.A., KOPPENWALLNER, G. and WUEST, W.,
Ein hypersonischer Windkanal für kleine Gasdichten in der Aerodynamischen Versuchsanstalt Göttingen.
Z. VDI Bd. 108, 1966, H. 35, p. 1733-1738.

[2] WUEST, W. and KOPPENWALLNER, G.,
The hypersonic low density wind tunnel of the AVA Göttingen - Operational behaviour and results on vibrational relaxation.
AIAA Paper No. 68-49, 1968.

[3] WUEST, W.,
Der hypersonische Vakuumwindkanal der Aerodynamischen Versuchsanstalt Göttingen (DFVLR).
To be publ. Jahrbuch 1969 of DGLR, Vieweg, Braunschweig 1970.

[4] BUETEFISCH, K.,
Experimentelle Bestimmung von Rotations- und Schwingungstemperatur und Dichte mit Hilfe der Elektronenstrahltechnik im Strömungsfeld eines hypersonisch angeströmten Kreiszylinders bei Stautemperaturen von 1 100 - 1 800 $^{\circ}$K.
DLR FB 69-63, 1969.

[5] KIENAPPEL, K.,
The influence of the geometric parameters of pressure tubes on static pressure measurement.
Pap. pres. at Euromech 18 Colloquium, 16-18 Sept. 1970, Southampton.

[6] KOPPENWALLNER, G.,
Experimentelle Untersuchung der Kräfte an einfachen Flugkörpern bei verdünnter Hyperschallströmung.
AVA-Report 69 A 40, Göttingen 1969.

[7] KOPPENWALLNER, G.,
Heat transfer to circular cylinders in hypersonic rarefied flow.
Pap. pres. at 7th Internat. Symposium on Rarefied Gas Dynamics, 29.6.-3.7.1970, Pisa.

[8] ROHDE, G.,
Galvanoplastisches Herstellungsverfahren dünnwandiger Modelle aus Nickel.
Z. Galvanotechnik 59, 1968, 5, p. 407-420.

[9] KOPPENWALLNER, G. and KIENAPPEL, K.,
Untersuchung der Druckverteilung, der Klappenmomente und des Strömungsfeldes an einem "Integralkörper" der Firma Junkers.
AVA Report 70 A 25, Göttingen 1970.

[10] KOPPENWALLNER, G., HEFER, G., WIDJAJA, I. and BOCK, J.,
Messungen an einem Lifting Body im Vakuumwindkanal der AVA und vergleichende Rechnungen.
Paper 70-031 pres. at DGLR Symposium Hyperschallströmungen, 4.6.1970, Hannover.

[11] LEGGE, H. and KOPPENWALLNER, G.,
Sphere measurements in a free jet and a hypersonic low density tunnel.
Pap. pres. at 7th Internat. Symposium on Rarefied Gas Dynamics, 29.6.-3.7.1970, Pisa.

[12] WUEST, W.,
Näherungsweise Berechnung von Kräften und Momenten in hypersonischer Strömung geringer Dichte.
AVA Report 70 A 17, Göttingen 1970.

[13] WIDJAJA, I., BAUNE, M., BOCK, J. and HASELOFF, J.,
Zur rechnerischen und experimentellen Ermittlung der aerodynamischen Beiwerte bei einem kompakten Wiedereintrittskörper.
Paper 69-036, DGLR Symposium Wiedereintritt von Raumflugkörpern, Köln, 16.10.1969.